

## Complex phase behavior of a fluid in slits with semipermeable walls modified with tethered chains

M. Borówko, A. Patrykiewicz, W. Rysko, S. Sokoowski, and J. Ilnytskyi

Citation: *J. Chem. Phys.* **134**, 044705 (2011); doi: 10.1063/1.3530791

View online: <http://dx.doi.org/10.1063/1.3530791>

View Table of Contents: <http://jcp.aip.org/resource/1/JCPSA6/v134/i4>

Published by the [American Institute of Physics](#).

---

### Related Articles

Molecular dynamics study of the processes in the vicinity of the n-dodecane vapour/liquid interface  
*Phys. Fluids* **23**, 112104 (2011)

The condensation and ordering of models of empty liquids  
*J. Chem. Phys.* **135**, 174903 (2011)

Molecular dynamics studies to understand the mechanism of heat accommodation in homogeneous condensing flow of carbon dioxide  
*J. Chem. Phys.* **135**, 064503 (2011)

Modulation of capillary condensation by trace component  
*AIP Advances* **1**, 022148 (2011)

Modeling of carbon dioxide condensation in the high pressure flows using the statistical BGK approach  
*Phys. Fluids* **23**, 052001 (2011)

---

### Additional information on *J. Chem. Phys.*

Journal Homepage: <http://jcp.aip.org/>

Journal Information: [http://jcp.aip.org/about/about\\_the\\_journal](http://jcp.aip.org/about/about_the_journal)

Top downloads: [http://jcp.aip.org/features/most\\_downloaded](http://jcp.aip.org/features/most_downloaded)

Information for Authors: <http://jcp.aip.org/authors>

### ADVERTISEMENT

**AIP**Advances

*Submit Now*

Explore AIP's new  
open-access journal

- Article-level metrics now available
- Join the conversation! Rate & comment on articles

## Complex phase behavior of a fluid in slits with semipermeable walls modified with tethered chains

M. Borówko,<sup>1</sup> A. Patrykiewicz,<sup>1</sup> W. Rżysko,<sup>1</sup> S. Sokołowski,<sup>1,a)</sup> and J. Ilnytskyi<sup>2</sup>

<sup>1</sup>*Department for the Modeling of Physico-Chemical Processes, Maria Curie-Skłodowska University, 20-031 Lublin, Poland*

<sup>2</sup>*Institute for Condensed Matter Physics, National Academy of Sciences of Ukraine, 1 Svientsitskii Street, 79011 Lviv, Ukraine*

(Received 25 August 2010; accepted 4 December 2010; published online 24 January 2011)

We study the phase behavior of a two-component fluid in a pore with the walls modified by tethered chains. The walls are completely permeable for one component of the fluid and completely impenetrable for the second component. The fluid is perfectly mixed in a bulk phase. We have found that depending on the details of the model the fluid undergoes capillary condensation inside the pore and wetting and layering transitions at the outer walls. Moreover, we have found transitions connected with the change of symmetry of the distribution of chains and fluid inside the pore. © 2011 American Institute of Physics. [doi:10.1063/1.3530791]

### I. INTRODUCTION

Fluids confined in pores exhibit significantly different physical behavior as compared with bulk systems. The competing fluid-pore walls and fluid–fluid interactions lead, under certain thermodynamic conditions, to surface-driven phase transitions, such as layering, wetting, and capillary condensation. To understand these phenomena, computer simulation techniques, as well as different theoretical methods are commonly used.<sup>1–3</sup>

The adsorbing properties of porous solids can be changed by their physical or chemical modification. This possibility is of practical importance and has been explored for several specific purposes. In particular, physical modification of the pore walls may be reached by preadsorption of certain molecules.<sup>4–7</sup> Experimentally important and theoretically interesting are the adsorbents in which the pore walls are modified by preadsorption of complex molecules, specifically by chains. The description of the microscopic structure and resulting thermodynamic properties of chain molecules grafted to the solid has attracted much attention.<sup>8–19</sup> This type of physical systems involves not only grafted species under confinement but also fluid particles that are adsorbed on the solid surfaces and within the layer of grafted molecules.

In our previous works<sup>20,21</sup> we used a density functional approach to discuss how tethering the chains to the walls of a slitlike pore can influence phase equilibria of confined fluids. Our research has been based on the application of a suitably modified version of the density functional theory, developed by Wu and co-workers.<sup>22–25</sup> We demonstrated that under certain thermodynamic conditions the pore filling may be accompanied by the change of the symmetry of the distribution of chains and confined fluid molecules inside the pore. Moreover, we also investigated<sup>26,27</sup> how chains grafted to a single surface modify the layering and wetting transitions and discussed the crossover between these two phenomena.

An interesting fact from the theoretical point of view model is based on the assumption that the wall (or walls of a pore) are completely impenetrable to some selected species of a fluid mixture, but permeable to other species.<sup>28–34</sup> Such models may be useful for interpreting the adsorption behavior of several natural systems as, for example, soils, in which not only adsorption but also absorption occurs. Therefore, it is of interest to consider a model of pores with partially permeable walls that would be useful in the interpretation of the results of experimental measurements of adsorption of fluids by some natural adsorbents, like clays or soils.

A system comprising of a layer of chain molecules terminally joined to a surface that is permeable only to some selected components of a fluid can be considered as a crude model of a membrane.<sup>35–42</sup> However, if two such layers are involved, the model can be used to mimic behavior of lipid bilayers that are of fundamental importance in cellular biology.<sup>43,44</sup> One of frequently considered models of bilayers is the so-called “tethered chain models,” according to which the bilayer integrity is maintained by tethering selected segments of chains to two common sheets.<sup>35,40,45–49</sup>

The aim of this work is to study the phase behavior of a two-component fluid in contact with a slitlike pore with walls modified by tethered chains. The walls are permeable for one component of the fluid and completely impenetrable for the second component. The fluid particles and the segments of chains interact via repulsive–attractive van der Waals forces. Therefore, the phase transitions we expect to find include: capillary condensation, layering and wetting. According to our knowledge, there exist no experimental works that would correspond exactly to the model considered by us. However, an interplay between capillary condensation and wetting in membranes has been proposed as a mechanism for dehumidification of streams in technological processes.<sup>50</sup> We are convinced that it is of interest to investigate phase transformations in such systems. To our best knowledge no such study, based on density functional approach has been presented so far.

<sup>a)</sup>Electronic mail: stefan.sokolowski@gmail.com.

For some model systems we also search for the symmetry change in the system.<sup>21</sup> The symmetry change was observed in the studies of surfactants confined in slits.<sup>51,52</sup> It was found that when two surfaces, coated with surfactant layers, were brought to a distance comparable to the surfactant length, the system can choose between having two compressed surfactant layers or having just one layer (attached to only one of the surfaces). We also note that spontaneous formation of asymmetric lipid bilayers by adsorption of vesicles was investigated by Wacklin and Thomas.<sup>53</sup> However, we should clearly state that the mechanism of the symmetry change discussed in the above quoted works was different from that studied in Ref. 21.

The paper is arranged as follows. In Sec. II we outline briefly the model and theory. Then, we first present comparisons of the theoretical results with selected Monte Carlo simulations and next—the results of theoretical calculations. Of course, the models considered do not exhaust all the situations that are possible to think of. In particular, we limit ourselves to studies of mixtures that do not exhibit demixing transitions in the bulk phase, therefore no surface demixing<sup>54–56</sup> of the fluid components is expected to occur. Moreover, we exclude from our considerations the Coulombic forces, which are known to play an important role in experimental setups and can also lead to several interesting phenomena.

## II. MODEL AND THEORY

We consider two walls, at a distance  $H$  apart, the first wall located at  $z = -H/2$  and the second at  $z = H/2$ . The walls are modified with tethered chains. For simplicity we assume that all the chains are identical and that each chain is built of  $M$  tangentially jointed hard spheres of the same diameter  $\sigma^{(c)}$ . The total number of chains is fixed. In the majority of the calculations presented below we have assumed that the number of chains pinned at each plane is the same. Under some conditions, however, this assumption has been removed. The chain connectivity is ensured by the binding potential between the nearest-neighbor segments. The total binding potential,  $V_b$ , is given by<sup>22–25</sup>

$$\exp[-\beta V_b(\mathbf{R})] = \prod_{i=1}^{M-1} \delta(|\mathbf{r}_i - \mathbf{r}_{i+1}| - \sigma^{(c)})/4\pi(\sigma^{(c)})^2. \quad (1)$$

In the above  $\mathbf{R} = (\mathbf{r}_1, \mathbf{r}_2, \dots, \mathbf{r}_M)$  is the vector of coordinates of all the segments of a given chain.

The chains are pinned by the first  $j = 1$ , segment, i.e., this segment feels a very strong, short-ranged, potential

$$\beta v_1^{(c)}(z) = -\mathcal{C}\delta(\kappa), \quad (2)$$

where  $\kappa = z + H/2$  for the first plane or  $\kappa = z - H/2$  for the second plane. In the above  $\mathcal{C}$  is a constant, the precise value of which is irrelevant if the total number of grafted chains is fixed.<sup>20,21,26,27,35</sup> All the remaining segments,  $j = 2, 3, \dots, M$  occupy the space  $Z_{1l} \leq z \leq Z_{1u}$  if the first segment is pinned at the first plane, and  $Z_{2l} \leq z \leq Z_{2u}$  for chains pinned at the second plane. To assure that, and taking into account the connectivity of the chains, we impose an ex-

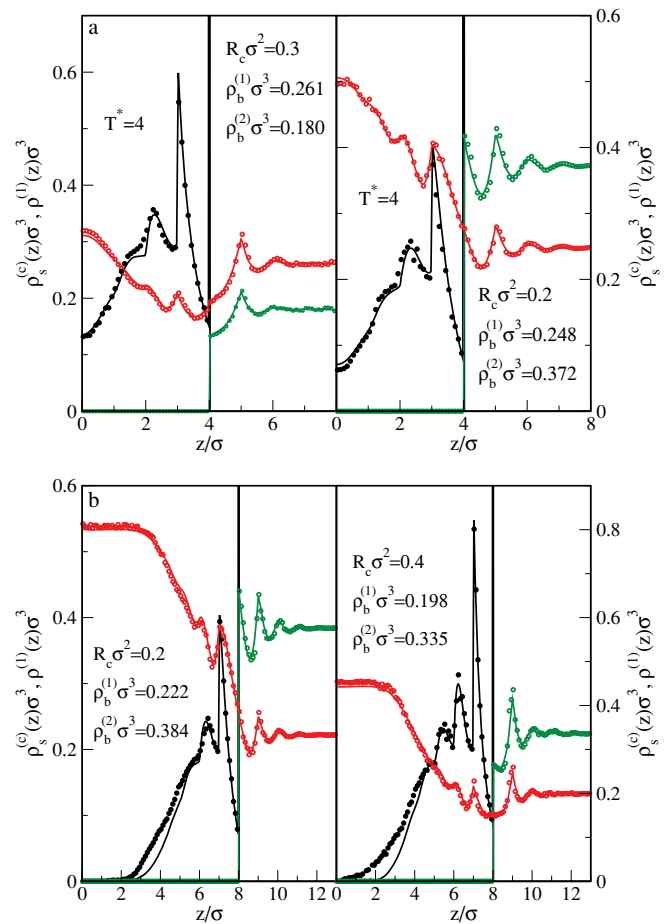


FIG. 1. A comparison of Monte Carlo (symbols) and density functional (lines) results. The calculations were carried out at  $T^* = 4$ , for chains composed of  $M = 8$  segments and for  $H = 8\sigma$  (part a) and  $H = 16\sigma$  (part b). The values of all remaining parameters are given in the figure.

ternal potential of the form

$$v_j^{(c)}(z) = \begin{cases} 0 & -H/2 \leq z < \min(H/2, -H/2 + M\sigma^{(c)}) \\ \infty & \text{otherwise} \end{cases}, \quad (3)$$

for the chains pinned at the first plane, and

$$v_j^{(c)}(z) = \begin{cases} 0 & \max(H/2, H/2 - M\sigma^{(c)}) \leq z < H/2 \\ \infty & \text{otherwise} \end{cases}, \quad (4)$$

for the chains pinned at the second wall. The illustration of the model used in this work, that is called “the inner leaflet model,” can be found in Fig. 1 of Ref. 35.

The system also contains spherical molecules of the species 1 and 2 of the diameters  $\sigma^{(1)}$  and  $\sigma^{(2)}$ , respectively. The molecules of the component 1 can be found anywhere in the system, thus the external potential acting on these molecules is zero everywhere,  $v^{(1)}(z) \equiv 0$ . However, the walls at  $z = \pm H/2$  are impenetrable for the species 2,

$$v^{(2)}(z) = \begin{cases} \infty & -H/2 \leq z \leq H/2 \\ 0 & \text{otherwise} \end{cases}, \quad (5)$$

i.e., the component 2 can be found only “outside” the pore formed by two walls. Note that similar definition of the potential was also used in previous works to model semipermeable walls.<sup>29,34,57</sup>

The interactions between all spherical species, i.e., the segments of chains ( $c$ ) and the species 1 and 2 are described by the Lennard-Jones (12,6) potentials

$$u_{ij}(r) = \begin{cases} 4\varepsilon^{(ij)}[(r/\sigma^{(ij)})^{12} - (r/\sigma^{(ij)})^6] & r \leq r_{\text{cut}}^{(ij)} \\ 0 & \text{otherwise} \end{cases}, \quad (6)$$

where  $i, j = 1, 2, c$ ,  $\sigma^{(ij)} = 0.5(\sigma^{(i)} + \sigma^{(j)})$ ,  $r_{\text{cut}}^{(ij)} = 3\sigma^{(ij)}$  is the cut-off distance and  $\varepsilon^{(ij)}$  are the energy parameters.

In order to proceed, let us introduce the following notation. The function  $\rho^{(c)}(\mathbf{R}) \equiv \rho^{(c)}(r_1, r_2, \dots, r_M)$  is the multidimensional distribution that describes the local density of chains. The functions  $\rho^{(i)}(\mathbf{r})$ ,  $i = 1, 2$  are the density distributions of spherical species. We also define the densities of individual segments,  $\rho_{sj}^{(c)}(\mathbf{r})$ , and the total segment density of chains,  $\rho_s^{(c)}(\mathbf{r})$  via the relations<sup>22–25</sup>

$$\rho_{sj}^{(c)}(\mathbf{r}) = \int d\mathbf{R} \delta(\mathbf{r} - \mathbf{r}_j) \rho^{(c)}(\mathbf{R}), \quad (7)$$

$$\rho_s^{(c)}(\mathbf{r}) = \sum_{j=1}^M \rho_{sj}^{(c)}(\mathbf{r}). \quad (8)$$

The system is studied in the grand canonical ensemble with the constraint on constancy of the number of chain molecules, i.e.,

$$R_C = \int_{Z_{1l}}^{Z_{2u}} \rho_{s1}^{(c)}(z) dz, \quad (9)$$

as it has already been mentioned. Moreover, when the condition of equal numbers of the chains pinned at each wall is imposed, then we additionally have

$$\int_{Z_{1l}}^{Z_{1u}} \rho_{s1}^{(c)}(z) dz = \int_{Z_{2l}}^{Z_{2u}} \rho_{s1}^{(c)}(z) dz. \quad (10)$$

The thermodynamic potential appropriate to describe the system is

$$\mathcal{Y} = F[\rho^{(c)}(\mathbf{R}), \rho^{(1)}(\mathbf{r}), \rho^{(2)}(\mathbf{r})] + \sum_{i=1}^2 \int d\mathbf{r} \rho^{(i)}(\mathbf{r}) (v^{(i)}(\mathbf{r}) - \mu) + \sum_{i=1}^M \int d\mathbf{r} \rho_{si}^{(c)}(\mathbf{r}) v_i^{(c)}(\mathbf{r}), \quad (11)$$

where  $F[\rho^{(c)}(\mathbf{R}), \rho^{(1)}(\mathbf{r}), \rho^{(2)}(\mathbf{r})]$  is the Helmholtz free energy functional.

The expression for  $F[\rho^{(c)}(\mathbf{R}), \rho^{(1)}(\mathbf{r}), \rho^{(2)}(\mathbf{r})]$  is taken from the theory outlined in previous works.<sup>20,21,26,27</sup> In particular, the hard-sphere contribution to the free energy functional was evaluated from the Boublik–Moonsori–Carnahan–Starling–Leland equation of state, cf. Ref. 23, assuming that the hard-sphere diameters are  $d^{(i)} = \sigma^{(i)}$ . To evaluate

the attractive force contribution to the free energy, a mean-field approximation was used and the potentials [Eq. (6)] were divided into repulsive and attractive parts according to the Weeks–Chandler–Anderson prescription (cf. Eq. (18) of Ref. 27).

The density profile  $\rho^{(i)}(\mathbf{r})$ ,  $i = 1, 2$  and the segment density profiles  $\rho_{si}^{(c)}(\mathbf{r})$  are obtained by minimizing the functional  $\mathcal{Y}$  under the constraint [Eq. (9)]. For the sake of brevity we do not present the resulting density profile equations, since they are formally identical with those reported in our recent works.<sup>20,21,26,27,35</sup>

The density profiles are used to calculate the adsorption isotherms. We distinguish the “inner,”  $\Gamma_i^{(i)}$ , and “outer,”  $\Gamma_o^{(i)}$ , isotherms of the component  $i = 1, 2$ , defined as

$$\Gamma_i^{(i)} = \int_{-H/2}^{H/2} dz [\rho^{(i)}(z) - \rho_b^{(i)}], \quad (12)$$

$$\Gamma_o^{(i)} = \int_{H/2}^{\infty} dz [\rho^{(i)}(z) - \rho_b^{(i)}], \quad (13)$$

where  $\rho_b^{(i)}$  is the bulk density of the component  $i$ . Strictly speaking,  $\Gamma_o^{(i)}$  is the excess isotherm calculated for the right-hand side of the pore  $\Gamma_o^{(i)} \equiv \Gamma_{or}^{(i)}$ . In some cases it might be useful to distinguish the right and left-hand side “outer” isotherms,  $\Gamma_{or}^{(i)}$  and  $\Gamma_{ol}^{(i)}$ , the latter defined by Eq. (13), but with the integration limits from  $-\infty$  to  $-H/2$ .

### III. RESULTS AND DISCUSSION

#### A. Comparisons with Monte Carlo data

In order to test the theory we have carried out comparisons with Monte Carlo simulation data. It is obvious, that when molecules interact via attractive–repulsive forces, the agreement of theory and simulations may crucially depend on the approximations used to determine the attractive force contribution to the free energy functional. Undoubtedly, the mean-field approximation does not allow to obtain a good quantitative agreement with simulation data within a wide range of densities and temperatures. Therefore, we have performed comparisons at high temperatures only.

The simulations were carried out assuming that the size of all spherical species (i.e., spherical molecules and the segments) is the same and equals  $\sigma^{(c)} = \sigma^{(1)} = \sigma^{(2)} \equiv \sigma$  and that  $\varepsilon^{(11)} = \varepsilon^{(12)} = \varepsilon^{(22)} = \varepsilon^{(c1)} = \varepsilon^{(c2)} \equiv \varepsilon$ . However, the segment–segment interaction was just of the hard-sphere type. The same model is next used in majority of theoretical calculations presented in Sect. III B.

Canonical ensemble Monte Carlo simulations were performed in a parallelepiped box of the dimensions  $XL \times XL \times ZL$ . The distance  $ZL$  was much larger than  $XL$ . The simulations were carried out using the Rosenbluths bias<sup>59</sup> for chains.

Figures 1(a) and 1(b) compare the results of the theory with Monte Carlo simulations. Figure 1(a) shows the results for the system where there is a remarkable partial overlap of the brushes attached to the opposite walls, whereas Fig. 1(b) for a wider pore.

In general, the agreement of simulations with theoretical predictions is satisfactory and comparable to that observed previously for the brushes attached to completely impenetrable walls. We must stress, however, that it does not mean that a similarly good agreement will be observed for other state conditions of the fluid; in particular, in the regions of possible phase transformations.

## B. Phase behavior

The phase behavior of the considered system depends on a number of parameters and for some combinations it may be quite complex. The main parameters of the model are the sizes of two types of spherical molecules and of the segments, the energy parameters defining the interactions between all the spherical species, the width of the pore, the number of tethered chains and their length, and the concentration of spherical molecules in the bulk phase. Moreover, the character of the distribution and some conditions delimiting the behavior of nonpinned segments may also be crucial. For example, one can consider the models in which the distribution of chains inside the pore is symmetric with respect to the pore center, or the models where the chains distribution is nonsymmetric.

The system contains a confined part (i.e., the part with the molecules placed inside the pore as well as located outside the pore, but near the pore walls) and a bulk part (containing the molecules located far away from the pore walls). Thus, we can expect the occurrence of different surface phase transitions (capillary condensation, wetting, and layering transitions), and the bulk phase transitions. Specific interactions between unlike species may lead to the demixing transition; in particular the demixing may occur in the outer surface layers.<sup>54–56</sup> Depending on the interactions between the spherical molecules and the segments of chains, additional demixing transitions may also occur inside the pore.

In order to reduce the number of possible situations to a minimum we consider an extremely simplified model that was used in simulations. In some cases, however, we allowed for  $\varepsilon^{(cs)}$  to be different from  $\varepsilon$ . This model excludes a possibility of demixing transition in the bulk phase. All the density functional calculations have been carried out assuming equimolar concentration of the bulk phase and in all cases we have assumed that the chains are built of  $M = 8$  segments. Despite so drastic limitations imposed on the model we shall demonstrate that its phase behavior may be quite complex.

Let us begin with the discussion of results for the systems exhibiting a symmetric distribution of chains inside the pore. In the present model we also assume that no segments are present outside the region of  $-H/2 \leq z \leq H/2$ , i.e., for the segments  $j = 2, 3, \dots, M$  we set  $\exp[-\beta v_j^{(c)}(z)] \equiv 0$  for  $z < -H/2$  and for  $z > H/2$ . The results displayed in Figs. 2 and 3 are for the systems characterized by the following parameters:  $H = 5\sigma$ ,  $R_c\sigma^2 = 0.2$  and  $\varepsilon^{(cs)} = \varepsilon$  and, as already mentioned, for the segment–segment interaction of hard-sphere type.

In Fig. 2 we show a series of adsorption isotherms of the component 1 inside (solid lines) and at one of the outer

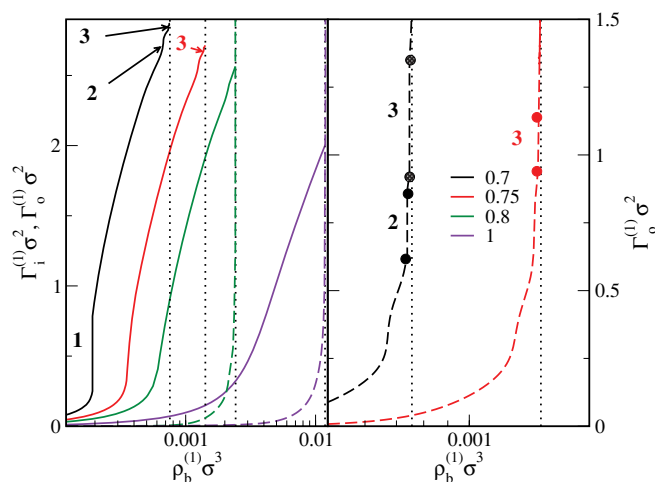


FIG. 2. Adsorption isotherms of the component 1 inside the pore (solid lines) and at one outer wall (dashed lines). Temperatures are marked by different colors, as indicated in the figure. Labels 1, 2, and 3 indicate the steps on the adsorption isotherms. Dotted vertical lines denote the bulk densities of the component 1 at the bulk liquid–vapor coexistence. The pore width is  $H = 5\sigma$ ,  $R_c = 0.2\sigma^2$ ; all remaining parameters are given in the text.

walls of the pore (dashed lines), evaluated at different temperatures. At  $T^* = kT/\varepsilon = 0.7$  we observe capillary condensation inside the pore (the step labeled as “1” on the adsorption isotherm in the left panel). At all remaining temperatures the pore filling is a continuous process. Performing additional calculations we have found that the critical temperature of capillary condensation is close to  $T_{cc}^* \approx 0.72$  in that system. It is significantly lower than the bulk critical temperature, which is equal to  $T_C^* \approx 1.37$ .

At higher temperatures the isotherms at the outer wall are continuous and diverge when the bulk density approaches the bulk liquid–vapor coexistence (marked as dotted, vertical lines in the right panel of Fig. 2). At lower temperatures, however, the “outer isotherms” exhibit steps (labeled as “2” and “3” in the right panel of Fig. 2), connected with a rapid filling of consecutive layers, i.e., with the layering transitions.

Figure 3 illustrates the changes in the system structure during the capillary condensation (part a) and layering transitions (part b). The left panel of Fig. 3(a) displays the changes in the total segment density profiles and in the profiles of the adsorbate 1 resulting from the capillary condensation, while the right panel shows how the distribution of selected individual segments changes when the fluid condenses inside the pore. Capillary condensation results in the formation of a pronounced peak of species 1 in the pore center. Instantaneously, the density of segments that are not chemically bonded to the walls decreases at the pore walls and increases in the inner part of the pore.

On the other hand, the layering transitions do not lead to remarkable changes of the structure inside the pore; only a small modifications of the density profile of the component 1 are seen in Fig. 3(b). However, these small changes lead to the occurrence of small jumps on the inner adsorption isotherms. They are hardly seen on the scale of Fig. 2(a), but their positions are indicated by the arrows with the labels “2” and “3.” These jumps on the outer adsorption result from the

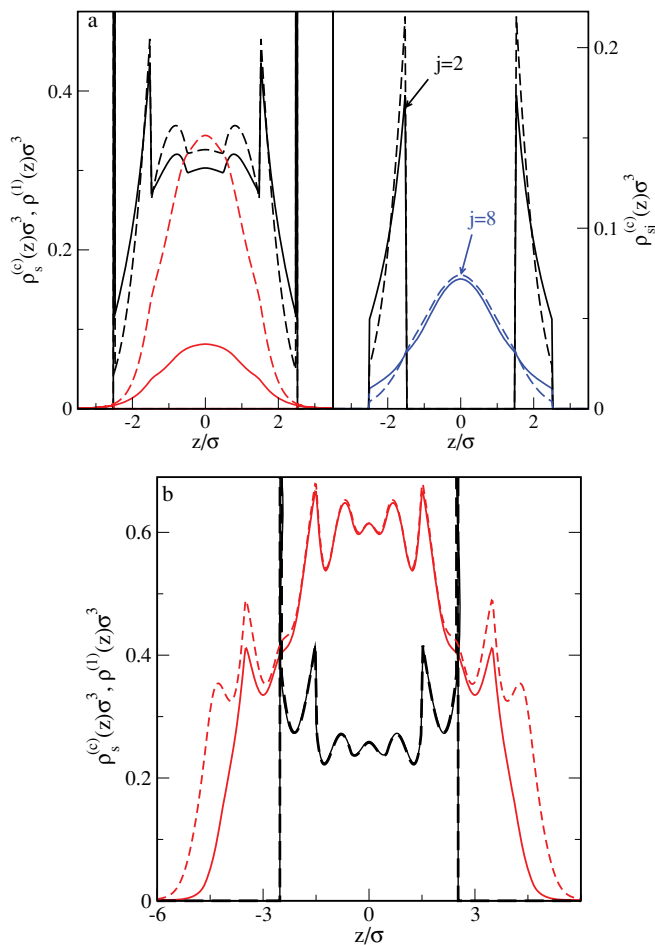


FIG. 3. (a) The change of the structure during capillary condensation at  $T^* = 0.7$ . (Left) The total segment density profiles (black lines) and the profiles of the component 1 (red lines). Solid and dashed lines show the profiles before and after capillary condensation (the jump on the adsorption isotherm in Fig. 2 marked as “1”). (Right) The profiles of the segments  $j = 2$  and  $8$ , as indicated in the figure. Similarly as in the left panel, solid and dashed line are the results evaluated before and after capillary condensation, respectively. (b) The change of the structure during the layering transition at  $T^* = 0.7$  marked as “2” in Fig. 2. Black lines are the total segment density profiles, while red lines— the profiles of the component 1. Solid lines denote the results before the transition, while dashed lines — after the transition. All the parameters are the same as in Fig. 2.

filling of the second and of the third layer outside the pore, respectively [cf. Fig. 3(b)]. The layering transition “2” vanishes at the temperature close to 0.72, while the transition “3” persists up to the temperature of  $T^* \approx 0.76$ . Thus, those temperatures are roughly the critical temperatures of layering transitions within the second and the third outer layers, respectively. The filling of the first layer has been found to be continuous within the investigated range of temperatures. Our calculations have also shown that at temperatures  $T^* \leq 0.75$ , and for the bulk densities very close to the bulk density at the liquid–vapor coexistence, the development of a thick film outside the pore occurs via a series of discontinuous steps. However, we have not explored this behavior in detail.

One can ask what is the origin of the layering transitions at the outer walls, if there is no attractive interaction potential between the wall and the spherical fluid components. However, there exist attractive chain’s segment-spherical fluid

particle forces, leading to the appearance of an effective attractive potential,  $v^{(\text{eff},i)}(z)$ ,  $i = 1, 2$  acting outside the pore walls,  $z > H/2$  or  $z < -H/2$ .

Because the structure of the chains between two walls changes very little during layering transitions, and because the layering transitions occur at bulk densities close to the bulk liquid–vapor coexistence, when the pore is almost completely filled with confined fluid whose density distribution  $\rho^{(1)}(z)$  for  $-H/2 < z < H/2$  is almost constant [cf. Fig. 3(b)], one can define an effective one-body potential  $v^{(\text{eff},i)}(z)$  acting on the molecules of species  $i = 1, 2$  outside the pore as

$$v^{(\text{eff},i)}(z) = 2\pi \int_{-H/2}^{H/2} dz' \left\{ \rho_s^{(e)}(z') \times \int_0^\infty u_{ci}(\sqrt{(|z-z'|^2 + r^2)}) r dr + \rho^{(1)}(z') \times \int_0^\infty u_{1i}(\sqrt{(|z-z'|^2 + r^2)}) r dr \right\}. \quad (14)$$

In the case considered here, the potential  $v^{(\text{eff},i)}(z)$  is strong enough to initiate the layering transitions at outer walls at low temperatures (the presentation of the plots of the potential  $v^{(\text{eff},i)}(z)$  has been omitted for the sake of brevity).

The tethered chains play a dual role. First, they act like obstacles reducing the volume inside the pore accessible to adsorbate molecules. The reduction of volume leads to the lowering of critical temperature of the confined fluid. Second, the segments of tethered chains attract the fluid particles. An increase of the density of segments inside the pore increases the attraction and therefore shifts the chemical potential in the transition point toward lower values. When the attractive interactions between the segments and fluid molecules are low enough, one expects to observe the effect of capillary evaporation rather than capillary condensation.

In Fig. 4 we show the examples of adsorption isotherms of the component 1 inside the pore of  $H = 5\sigma$  wide and at one of its outer walls. In part a of Fig. 4 all the parameters, but  $R_C$ , which is now 0.1, are the same as in Figs. 2 and 3. We have not observed capillary condensation over the entire range of temperatures used. At still lower temperatures a capillary evaporation has been seen instead, but we did not perform detailed studies. Also, the outer isotherms,  $\Gamma_o^{(1)}$ , remain low and finite up to the bulk liquid–vapor coexistence at all temperatures used. This means that the outer surfaces are not wetted by the adsorbate. However, when the model parameters are slightly altered by setting  $\varepsilon^{(1)} = \varepsilon^{(2)} = 1.5\varepsilon$ , the picture of phase transformations in the system changes. The capillary condensation [Fig. 4(b)] occurs up to  $T^* \approx 0.92$ , the outer surface is wetted [Fig. 4(c)] and at the lowest temperature we also observe layering transitions. The adsorption jump associated with the layering transition within the second outer layer is distinguished by two delimiting black dots in Fig. 4(c).

We recall that in the case of the isotherms displayed in Fig. 2 the layering transitions induce the occurrence of small jumps on the isotherms  $\Gamma_i^{(1)}$  inside the pore. This means that the thick film growing outside the pore “pushes” some molecules into the pore. Here we observe a different phenomenon. When capillary condensation occurs, an abrupt

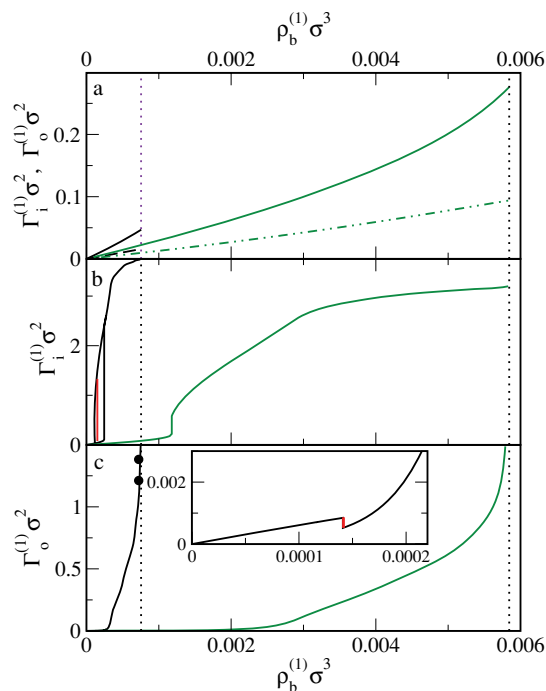


FIG. 4. (a) Isotherms  $\Gamma_i^{(1)}$  (solid lines) and  $\Gamma_o^{(1)}$  (dashed and dash-dotted lines); the values of  $\Gamma_o^{(1)}$  are multiplied by 8) at  $T^* = 0.7$  (black) and 0.9 (green), evaluated for  $R_c\sigma^2 = 0.1$ . The values of all remaining parameters are the same as in Figs. 2 and 3. (b) and (c) Isotherms  $\Gamma_i^{(1)}$  (b) and  $\Gamma_o^{(1)}$  (c). Now  $\varepsilon^{(cs)} = 1.5\varepsilon$ ,  $s = 1, 2$ , but all remaining parameters are the same as in (a). Solid lines are the results at  $T^* = 0.7$  and green lines—at  $T^* = 0.9$ . In the case of  $\Gamma_i^{(1)}$  at  $T^* = 0.7$  we show hysteresis loop and the red lines denote the equilibrium transition. The inset in (c) illustrates the behavior of  $\Gamma_o^{(1)}$  at  $T^* = 0.7$  within the region of the capillary condensation shown in (b). Dotted vertical lines denote the bulk density of the component 1 at the liquid–vapor coexistence.

filling of the pore by a liquid-like phase causes a (small) decrease of adsorption outside the pore. This is also illustrated in Fig. 5, where in the left panel we have plotted the density profiles corresponding to the dilute and dense phases inside the pore. The right panel, however, shows the individual density profiles of selected segments  $j$ . For a better visualization we have magnified a part of the profiles of the fluid component 1 in the region close to the pore wall.

The capillary condensation results in the formation of a “droplet” of species 1 close to the pore center. This process is accompanied by a shift of the segments of tethered chains in the same direction, i.e., it leads to the chains straightening. Due to the existence of chemical bonds between the nearest segments, the segments of chains inside the pore are more ordered than the molecules of fluid 1. When the droplet is formed, the molecules of fluid 1 are “sucked into” the pore from the space outside the pore, (cf. the inset to the right panel of Fig. 5), what results in the lowering of the isotherm  $\Gamma_o^{(1)}$ , see the inset to Fig. 4(c).

The next series of calculations has been carried out setting  $R_c\sigma^2 = 0.4$ . The results in Fig. 6 are for  $\varepsilon^{(c1)} = \varepsilon^{(c2)} = 0.8\varepsilon$  (parts a and b) and for  $\varepsilon^{(c1)} = \varepsilon^{(c2)} = \varepsilon$  (part c). All remaining parameters are the same as in all preceding figures. Now, the density of segments is very high inside the pore, so that no capillary condensation is observed neither for

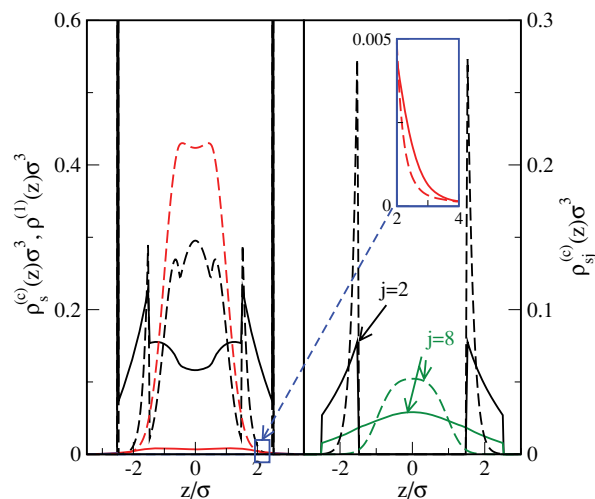


FIG. 5. (Left) The changes in the structure of the total segment density profiles (black lines) and of the component 1 (red lines) during the capillary condensation. (Right) The changes of segment density profiles of the segments  $j = 2$  and 8. The inset magnifies the component 1 density profiles within the region marked in the left panel by a blue box. In both panels the structure before and after the condensation is marked by solid and dashed lines, respectively. The calculations are for the system shown in Figs. 4(b) and 4(c) at  $T^* = 0.7$ .

$\varepsilon^{(c1)} = \varepsilon^{(c2)} = \varepsilon$  nor for  $\varepsilon^{(c1)} = \varepsilon^{(c2)} = 0.8\varepsilon$  within the investigated range of temperatures,  $T^* \geq 0.7$ . When  $\varepsilon^{(c1)} = \varepsilon^{(c2)} = \varepsilon$  (part c) the  $\Gamma_o^{(1)}$  isotherms behave like those in Fig. 2 and at  $T^* = 0.8$  we observe the existence of layering transitions. The transition within the second outer layer is marked by dots in Fig. 6(c). The layering jump also induces the jump of the

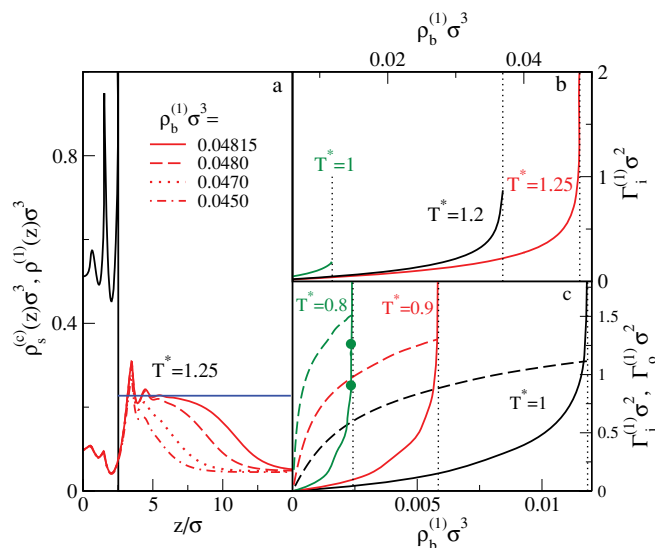


FIG. 6. The results obtained for  $R_c\sigma^2 = 0.4$  and  $\varepsilon^{(c1)} = \varepsilon^{(c2)} = 0.8\varepsilon$  (a and b) and  $\varepsilon^{(c1)} = \varepsilon^{(c2)} = \varepsilon$  (c). All remaining parameters used in the calculations were the same as in the preceding figures. (a) The growth of the wetting film at  $T^* = 1.25$ . The bulk fluid densities are given in the figure. The total segment density profiles are displayed as black curve; the profiles obtained for different  $\rho_b^{(1)}$  are indistinguishable on the figure scale. The horizontal blue line denotes the bulk dew density. (b) The isotherms  $\Gamma_o^{(1)}$  at three temperatures, while (c)—the isotherms  $\Gamma_o^{(1)}$  (solid lines) and  $\Gamma_i^{(1)}$  (dashed lines) also at three selected temperatures. Dotted vertical lines in (b) and (c) denote the bulk densities at the liquid–vapor coexistence.

“inner” adsorption isotherm, but it is invisible on the figure scale. With the increase in temperature, the layerings are rounded out and the isotherms  $\Gamma_o^{(1)}$  have the shape characteristic for a complete wetting.

However, when  $\varepsilon^{(c1)} = \varepsilon^{(c2)} = 0.8\varepsilon$ , i.e., when the segment-fluid interactions are weaker (and the effective potential  $v^{(eff,i)}(z)$  is also weaker), the situation changes, see Fig. 6(b). Again, we do not observe any trace of capillary condensation, but now at lower temperatures ( $T^* = 1$  and  $T^* = 1.2$ ), the adsorption  $\Gamma_o^{(1)}$  remains finite up to the bulk liquid–vapor coexistence, whereas at  $T^* = 1.25$  the isotherm  $\Gamma_o^{(1)}$  diverges when the bulk density approaches the bulk liquid–vapor coexistence. Thus, what we have here is the wetting transition. We have carried out several calculations at the temperatures from the range  $1.2 \leq T^* < 1.25$  and have not found the prewetting transition. Therefore, the wetting in the system in question is likely to be the second order transition.

Figure 6(a) illustrates the growth of the film outside the pore at  $T^* = 1.25$ . We see that the thickness of the film grows continuously when the density approaches the bulk liquid–vapor coexistence ( $\rho_b^{(1)}\sigma^3 = 0.04825$ ), while the total segment density profiles, and also the profiles of individual segments (the relevant plot has been omitted for the sake of brevity), remain practically unchanged. The blue horizontal line in Fig. 6(a) denotes the bulk dew density, which is approached by the density of growing film.

All the calculations presented so far have been carried out for  $H = 5\sigma$ . For narrow pores (compared with the maximum length of chains,  $M\sigma$ ), there is a strong overlap of brushes attached to opposite walls. When  $H$  is large compared with  $M\sigma$ , the adsorption at the brushes attached to opposing walls becomes almost independent. Under such conditions one can expect the occurrence of phase transitions similar to those discussed in Refs. 26 and 27 in addition to the capillary condensation (evaporation). As we have learnt from the results presented above, the transitions occurring at the outer walls, however, depend mainly on the amount of attached segments,  $R_c$ , and on the strength of the fluid–segment interactions. Therefore, the most interesting are the cases when  $H$  is not too big, since in those cases a competition between different effects may lead to novel phenomena.

In Fig. 7 we show examples of the results for the system characterized by the following set of parameters:  $H = 12\sigma$ ,  $R_c\sigma^2 = 0.6$  and  $\varepsilon^{(c1)} = \varepsilon^{(c2)} = \varepsilon$ . Similarly as in previously considered model, the segment–segment interaction is of hard-sphere type. For the system under study the capillary condensation critical temperature is close to 1.069, i.e., the isotherm  $\Gamma_i^{(1)}$  at  $T^* = 1.07$  is only marginally supercritical. The phase diagram for the capillary condensation, plotted in the temperature–adsorption plane is displayed in the inset of Fig. 7(a). At  $T^* = 0.8$  we have evaluated the onsets and terminating points of two layering transitions (within the second and the third outer layers), and of the layering transition within the third layer at  $T^* = 0.9$ . Undoubtedly, at lower temperatures the layering transitions extend over higher layers as well, but we did not explore this phenomenon in details.

At the chemical potential below the capillary condensation, the most inner part of the pore is unfilled and the fluid molecules adsorb “inside” the brush. Capillary condensation

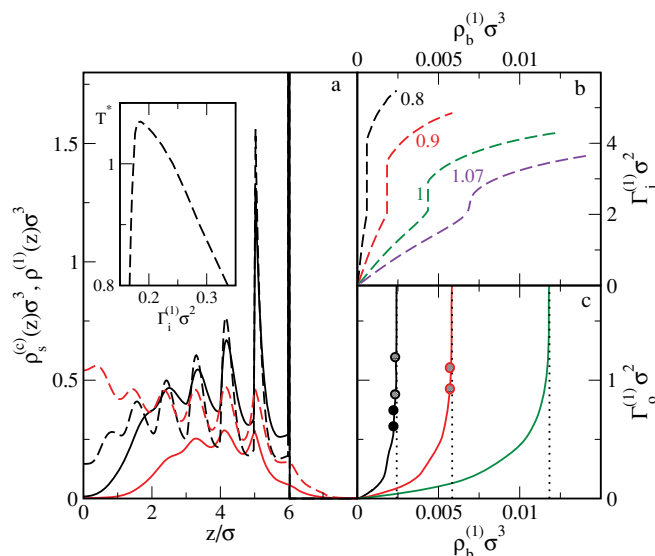


FIG. 7. The results for the system with  $H = 12\sigma$  and  $R_c\sigma^2 = 0.6$  (the values of all remaining parameters are given in the text). (a) A comparison of the structures at  $T = 0.8$  (only a half of the profiles is displayed) before ( $\rho_b^{(1)}\sigma^3 = 0.00044$ , solid lines) and after ( $\rho_b^{(1)}\sigma^3 = 0.001$ , dashed lines) the capillary condensation. Total segment density profiles are in black, while the component 1 profiles are in red. (b) The isotherm  $\Gamma_i^{(1)}$  at the temperatures given by the numbers in the figure, while (c)—the isotherms  $\Gamma_o^{(2)}$ . The meaning of colors in (b) and (c) is the same. The dots in (c) make the adsorption steps more visible. (a) shows the adsorption–temperature phase diagram for the capillary condensation transition.

leads to the filling of the pore interior by a fluid and causes the brush straightening. A high density of chain segments inside the pore leads to the development of a rather well ordered structure of the brush, in which the chains order in the direction perpendicular to the walls. Because the size of the molecules 1 is the same as the size of the segments, the ordering of the adsorbate follows the brush ordering and development of a layered structure, cf. Fig. 7(a).

Finally, we remove the assumption about symmetric distribution of tethered chains inside the pore, that was *a priori* imposed in all previous calculations. Of course, the total amount of tethered chains is still fixed, but now their distribution (and the distribution of their tethered “heads” in particular) at the two walls can be different. The shape of the local density functions results from the minimization of the thermodynamic potential  $\mathcal{Y}$  [Eq. (11)]. In that model the minimization may either lead to symmetric or to non-symmetric distribution of the fluid in the system. In particular, under certain thermodynamic conditions we can expect the symmetry change in the system: from the profiles symmetric with respect to the pore center to the nonsymmetric profiles (or vice versa). We recall that in the case of a similar model, but used to describe adsorption inside the pore with totally impenetrable walls, we observed such changes of the distributions of both the tethered chains and the confined fluid.<sup>21</sup>

The model used in calculations is described by the following set of parameters:  $H = 6.5\sigma$ ,  $R_c\sigma^2 = 0.2$ , and  $\varepsilon^{(c1)} = \varepsilon^{(c2)} = \varepsilon$ , and the results are presented in Fig. 8. Let us analyze the adsorption  $\Gamma_i^{(1)}$  at  $T^* = 0.8$ , cf. Fig. 8(a). There

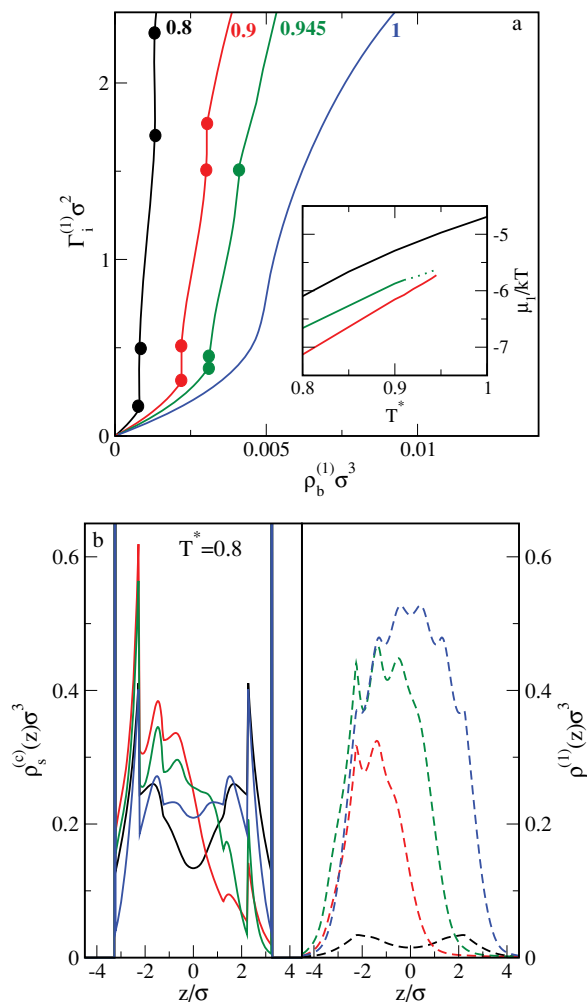


FIG. 8. (a) The isotherms  $\Gamma_i^{(1)}$  at the temperatures given in the figure. Dots delimit the adsorption jumps. (b) The total segment density profiles (left panel, solid lines) and the profiles of component 1 (right panel, dashed lines) at  $T^* = 0.8$ . Colors denote the bulk densities of component 1: black— $\rho_b^{(1)}\sigma^3 = 0.0008$ ; red— $\rho_b^{(1)}\sigma^3 = 0.0009$ ; green— $\rho_b^{(1)}\sigma^3 = 0.0013$ ; and blue— $\rho_b^{(1)}\sigma^3 = 0.0014$ . The inset to (a) displays the phase diagram in the temperature–chemical potential of fluid “1” plane. Black line is a part of the bulk diagram, red line denotes a partial filling and the symmetry change while green line—the final pore filling and return to the symmetric density profiles.

are two jumps of  $\Gamma_i^{(1)}$ , delimited by black dots. To interpret these steps we inspect the density profiles given in Fig. 8(b). At low bulk densities  $\rho_b^{(1)}$  the profiles of segments and of the component 1 are symmetric with respect to the pore center. After the first jump of  $\Gamma_i^{(1)}$  the symmetry of the profiles is broken. The adsorption  $\Gamma_i^{(1)}$  increases abruptly, but the adsorbate molecules accumulate in the part of the pore where the density of segments is high. A further increase of  $\rho_b^{(1)}$  diminishes slowly the asymmetry of local density distributions, and finally at a certain bulk density the system abruptly (the second jump in adsorption) returns to the symmetric local densities. Similar changes are observed at  $T^* = 0.9$ , but both adsorption steps become smaller. At  $T^* = 0.945$  the first step, although very small, still exists. However, instead of the second step we observe a “knee” on the isotherm.

We have inspected the behavior of the system at the temperatures from the range  $0.9 < T^* < 0.95$  and plotted the phase diagram in the chemical potential–temperature plane, cf. the inset to Fig. 8(a). The black line denotes a part of the bulk phase diagram, and the red line displays the first transition connected with the instantaneous partial filling of the pore accompanied by symmetry breaking. This transition occurs at the temperatures up to about 0.95. The green line corresponds to a final filling of the pore and the return to the symmetric distributions. However, it is difficult to determine precisely the temperature at which the jump of adsorption transforms into the knee, presumably it occurs at  $T^* \approx 0.91$ . At the temperature of  $T^* = 0.95$  we have not seen any changes in the symmetry during the adsorption. In Fig. 8(a) we have also plotted the isotherm at  $T^* = 1$ . It is smooth and no changes in the character of the distribution of the chains as well as of the fluid particles in the pore occurs in this case.

The sequence of transitions in the system under study is as follows. At low temperatures and for low enough bulk fluid densities the pore is filled with a rarefied fluid. The density profiles of the fluid and the chains are symmetric. At a certain bulk density the pore is abruptly partially filled and this transformation is accompanied by the change of the local densities from symmetric to nonsymmetric. Then, a second transformation takes place. It is connected with the filling of the entire pore and with the “return” of the system to symmetric local densities.

The explanation for the observed changes is as follows. The value of the thermodynamic potential  $\mathcal{Y}$  in a given thermodynamic state results from an interplay between the terms arising from hard-sphere interactions, chain connectivity and attractive interactions. The latter term attains its minimum for maximum attraction between spherical species. The attractive interactions tend to increase the density in the system. If a constraint on constancy of the amount of some species is imposed, the increase of the contribution to the free energy due to attractive interactions may occur via appearance of less and more dense regions that, in the case of the system under study, results in the breaking of the density profiles symmetry. On the other hand, a further increase of the density, due to the confinement of spherical molecules of species “1,” leads to a significant increase of the volume exclusion (hard-sphere) contribution to the excess free energy. An interplay between these free energy terms causes that and when the density of fluid between the walls is high enough, the local densities become symmetric again.

The transitions described above resemble those in a pore with impenetrable walls.<sup>21</sup> However, unlike in our previous study, here we have not observed the symmetry changes in the systems containing tethered chains alone. Of course, this difference is a consequence of differences in the models used. Namely, in the previous work, the Lennard-Jones segment–segment interactions were assumed, while in the present work we have imposed hard-sphere interactions between segments. When attractive segment–segment interactions exist, an interplay between different contributions to the free energy functional can lead to nonsymmetric distribution of tethered chains inside the pore. This is not possible in the case of

hard-sphere segment–segment interactions, because the negative contribution to the free energy due to chain connectivity is too small, even for long chains.

One can ask whether the discussed transformations are not artifacts of the theory. However, our previous findings<sup>21</sup> were qualitatively confirmed, partially at least, by computer simulations.<sup>59</sup> Also note that the change from symmetric to nonsymmetric density profiles was also observed and discussed in details in the case of density functional studies of adsorption of spherical molecules confined in carbon-like pores.<sup>60</sup> Moreover, the breaking of the symmetry of density profiles was also found in the case of adsorption of mixtures in pores.<sup>56,61</sup>

#### IV. CONCLUSIONS

Let us briefly summarize our observations. The model calculations presented above have demonstrated that even in the case of such simple systems as those considered by us the phase behavior may be quite complex and depends on the details of the model. If the symmetry of the local densities with respect to the plane  $z = 0$  is imposed, then the capillary condensation inside the pore as well as the layering or wetting transitions at the outer pore walls occur. In none of the cases investigated we have found a prewetting transition and only the second-order wetting was observed. The layering transitions have also been found to affect the “inner” adsorption isotherm. Each layering transition causes a small discontinuous jump at the inner adsorption isotherm. However, the capillary condensation has been found to result in a small discontinuous decrease of adsorption at the outer adsorption isotherm. When the condition of symmetric distribution of chains between the walls is removed, we have also found the transitions connected with the change of symmetry of density profiles. An initially symmetric distribution of chains and spherical components changes to a nonsymmetric one, with a “mixture” of pinned chains and adsorbate molecules grouped at one wall. A further increase of the bulk gas density has been found to lead to the re-entrance of symmetry and the pore filling. This situation is different from the changes observed previously<sup>21</sup>, where the segment–segment interaction was of the Lennard-Jones type. In the latter case a nonsymmetric distribution was also observed for systems involving no spherical molecules of fluid species.

All our calculations were carried out using a mean-field approximation to calculate the contribution of the free energy resulting from attractive interactions. We are aware that this approach is a crude approximation, and that the approaches based on the so-called first-order mean spherical approximation (FMSA),<sup>62</sup> combined with the fundamental measure theory are more accurate for one-component nonuniform fluids.<sup>63</sup> Although the FMSA was also developed for bulk mixtures,<sup>64</sup> it has not yet been implemented to investigate nonuniform fluid mixtures nor any comparison with simulation results has been given. Instead of FMSA, a mean-field type approach with the mean-field attractive contribution to the free energy weighted by a certain factor has been employed to describe nonuniform mixtures, cf. Ref. 65.

Our calculations have been carried out for a very simple model. In particular, we have assumed the same sizes of all spherical species and a complete mixing in the bulk phase. Of course, the phase behavior is expected to be much richer when the demixing transition in the bulk phase takes place. Another enrichment of the phase behavior is expected for the chains build of segments exhibiting different properties (e.g., diblock copolymers). However, the proposed approach can be also extended to the case when electrostatic interactions are present. This can be done by modifying the theory along the lines described in Ref. 66 We already know (see, e.g., Ref. 67) that for some systems containing ions in contact with a lipid bilayer unexpected effects of ions on the structural and electrical properties of the membrane can be observed. This problem is currently under study in our laboratory.

#### ACKNOWLEDGEMENTS

This work was supported by the Ministry of Science of Poland under the Grant No. N N204 151237. J.I. acknowledges support from EC under Grant No. IRSES 268498.

- <sup>1</sup>L. D. Gelb, K. E. Gubbins, R. Radhakrishnan, and M. Śliwinski-Bartkowiak, *Rep. Prog. Phys.* **62**, 1573 (1999).
- <sup>2</sup>M. Schoen and S. Klapp, in *Reviews in Computational Chemistry*, edited by K. B. Lipkowitz, T. R. Cundari, and D. B. Boyd (Wiley-VCH, Hoboken, 2007), Vol. 24.
- <sup>3</sup>P. Bryk, K. Bucior, S. Sokołowski, and G. Żukocinski, *J. Phys. Chem. B* **109**, 2977 (2005).
- <sup>4</sup>R. Mahboub, Y. Elmouzdahir, A. Elmchaouri, A. Carvalho, M. Pinto, and J. Pires, *Colloids and Surfaces A* **280**, 81 (2006).
- <sup>5</sup>L. Zhou, X. W. Liu, J. W. Li, Y. Sun, and Y. P. Zhou, *Colloids Surf., A* **273**, 117 (2006).
- <sup>6</sup>C. Knöfel, J. Descarpentries, A. Benzaouia, V. Zelenak, S. Mornet, P. L. Llewellyn, and V. Horneb eqq, *Microporous Mesoporous Mater.* **99**, 79 (2007).
- <sup>7</sup>C. Drummond and J. Jsrachvili, *J. Pet. Sci. Eng.* **45**, 61 (2004).
- <sup>8</sup>C. Pastorino, K. Binder, T. Keer, and M. Muller, *J. Chem. Phys.* **124**, 064902 (2006).
- <sup>9</sup>S. K. Pattanayek, T. T. Pham, and G. G. Pereira, *J. Chem. Phys.* **122**, 214908 (2005).
- <sup>10</sup>F. Fang and I. Szleifer, *Proc. Natl. Acad. Sci. U.S.A.* **103**, 5769 (2006).
- <sup>11</sup>M. Friedel, A. Baumketner, and J.-E. Shea, *J. Chem. Phys.* **126**, 095101 (2007).
- <sup>12</sup>D. Dimitrov, A. Milchev, and K. Binder, *J. Chem. Phys.* **125**, 034905 (2006).
- <sup>13</sup>D. I. Dimitrov, A. Milchev, K. Binder, and D. W. Heermann, *Macromol. Theory Simul.* **15**, 573 (2006).
- <sup>14</sup>A. G. Koutsoubas, N. Spiliopoulos, D. L. Anastassopoulos, A. A. Vradis, and C. Toprakcioglu, *J. Chem. Phys.* **131**, 044901 (2009).
- <sup>15</sup>R. Serna-Guerrero and A. Sayari, *Chem. Eng. J.* **161**, 182 (2010).
- <sup>16</sup>A. Milchev, S. A. Egorov, and K. Binder, *J. Chem. Phys.* **132**, 184905 (2010).
- <sup>17</sup>J. L. Rafferty, J. I. Siepmann, and M. R. Schure, *J. Chromatogr. A* **1216**, 2320 (2009).
- <sup>18</sup>S. Jain, V. V. Ginzburg, P. Jog, J. Weinhold, R. Srivastava, and W. G. Chapman, *J. Chem. Phys.* **131**, 044908 (2009).
- <sup>19</sup>J. L. Suter, R. L. Anderson, H. C. Greenwell, and P. V. Coveney, *J. Mater. Chem.* **19**, 2482 (2009).
- <sup>20</sup>O. Pizio, A. Patrykiewicz, and S. Sokołowski, *J. Phys. Chem. C* **111**, 15743 (2007).
- <sup>21</sup>O. Pizio, M. Borówko, W. Rzyśko, T. Staszewski, and S. Sokołowski, *J. Chem. Phys.* **128**, 044702 (2008).
- <sup>22</sup>Y. -X. Yu and J. Wu, *J. Chem. Phys.* **117**, 2368 (2002).
- <sup>23</sup>Y. -X. Yu and J. Wu, *J. Chem. Phys.* **118**, 3835 (2003).
- <sup>24</sup>D. P. Cao and J. Wu, *Langmuir* **22**, 2712 (2007).
- <sup>25</sup>X. Xu and D. Cao, *J. Chem. Phys.* **131**, 054901 (2009).

- <sup>26</sup>A. Patrykiewicz, S. Sokołowski, R. Tscheliessnig, J. Fischer, and O. Pizio, *J. Phys. Chem. B* **112**, 4552 (2008).
- <sup>27</sup>M. Borówko, A. Patrykiewicz, S. Sokołowski, and T. Staszewski, *Collect. Czech. Chem. Commun.* **75**, 221 (2010).
- <sup>28</sup>P. Marsh, G. Rickayzen, and M. Celleja, *Mol. Phys.* **84**, 799 (1995).
- <sup>29</sup>P. Bryk, A. Patrykiewicz, J. Reszko-Zygmunt, and S. Sokołowski, *Mol. Phys.* **96**, 1509 (1999).
- <sup>30</sup>S. Murad and J. Powles, in *Computational Methods in Surface and Colloid Science*, edited by Marcel Borówko (Marcel Dekker, New York, 2000), Chap. XVI.
- <sup>31</sup>P. Bryk, J. Reszko-Zygmunt, W. Rżysko, and S. Sokołowski, *Mol. Phys.* **98**, 117 (2000).
- <sup>32</sup>M. Schmidt, A. Fortini, and M. Dijkstra, *J. Phys.: Condens. Matter* **16**, S4159 (2004).
- <sup>33</sup>A. Fortini, M. Schmidt, and M. Dijkstra, *Phys. Rev. E* **73**, 051502 (2006).
- <sup>34</sup>Z. Yang, X. Yang, and Z. Xu, *J. Membr. Sci.* **320**, 381 (2008).
- <sup>35</sup>A. Patrykiewicz, S. Sokołowski, J. Ilnytskiy, and Z. Sokołowska, *J. Chem. Phys.* **132**, 244704 (2010).
- <sup>36</sup>P. van der Ploeg and H. J. C. Berendsen, *J. Chem. Phys.* **76**, 3271 (1982).
- <sup>37</sup>M. Milik, A. Kolinski, and J. Skolnick, *J. Chem. Phys.* **93**, 4440 (1990).
- <sup>38</sup>N. Zheng, J. Geehan, and M. D. Whitmore, *Phys. Rev. E* **75**, 051922 (2007).
- <sup>39</sup>C. Ren and Y. Ma, *Phys. Rev. E* **80**, 011910 (2009).
- <sup>40</sup>A. L. Frischknecht and L. J. D. Frink, *Phys. Rev. E* **72**, 041923 (2005).
- <sup>41</sup>G. van Meer, D. R. Voelker, and G. W. Feigenson, *Nat. Rev. Mol. Cell Biol.* **9**, 112 (2008).
- <sup>42</sup>R. E. Kesting and A. K. Fritzsche, *Polymeric Gas Separation Membranes* (Wiley, New York, 1993), pp. 61–233.
- <sup>43</sup>H. T. Tien and A. Ottova-Leitmannova, *Planar Lipid Bilayers (BLMs) and Their Applications* (Elsevier, Amsterdam, 2003).
- <sup>44</sup>A. L. Frischknecht and L. J. D. Frink, in *Biomembrane Frontiers: Nanostructures, Models, and the Design of Life*, edited by R. Faller, T. Jue, M. L. Longo, and S. H. Risbud, (Humana, Dordrecht, 2009), Vol. 2.
- <sup>45</sup>M. Bloom, E. Evans, and O. G. Mouritsen, *Q. Rev. Biophys.* **24**, 293 (1991).
- <sup>46</sup>A. Ben-Shaul, I. Szleifer, and W. M. Gelbart, *J. Chem. Phys.* **83**, 3597 (1985).
- <sup>47</sup>I. Szleifer, A. Ben-Shaul, and W. M. Gelbart, *J. Chem. Phys.* **85**, 5345 (1986); **86**, 7094 (1987).
- <sup>48</sup>T. Sintes and A. Baumgartner, *Physica A* **249**, 571 (1998).
- <sup>49</sup>L. Whitehead, C. M. Edge, and J. W. Essex, *J. Comput. Chem.* **22**, 1622 (2001).
- <sup>50</sup>G. Ceve, H. Richardsen, and A. Welland-Waibel, U.S. Patent 7,591,949B2 (September 22, 2009); A. S. Kesten, S. Satyapal, J. N. Blechner, and C.-Y. A. Tsai, R. Jarvis, U.S. patent No. 2002/0139245 A1 (2002).
- <sup>51</sup>F. A. M. Leermakers, L. K. Koopal, T. P. Goloub, A. W. P. Vermeer, and J. Kijlstra, *J. Phys. Chem B* **110**, 8756 (2006).
- <sup>52</sup>F. A. M. Leermakers, L. K. Koopal, W. J. Lokar, and W. A. Ducker, *Langmuir* **21**, 11534 (2005).
- <sup>53</sup>H. P. Wacklin and R. K. Thomas, *Langmuir* **23**, 7644 (2007).
- <sup>54</sup>A. Martinez, O. Pizio, A. Patrykiewicz, and S. Sokołowski, *J. Phys. Condens. Matter* **15**, 2269 (2003).
- <sup>55</sup>K. Bucior, A. Patrykiewicz, O. Pizio, and S. Sokołowski, *Mol. Phys.* **101**, 1477 (2003).
- <sup>56</sup>A. Patrykiewicz, O. Pizio, S. Sokołowski, and Z. Sokołowska, *Phys. Rev. E* **69**, 061605 (2004).
- <sup>57</sup>P. Bryk, S. Sokołowski, and O. Pizio, *J. Phys. Chem. B* **103**, 3366 (1999).
- <sup>58</sup>M. N. Rosenbluth and A. W. Rosenbluth, *J. Chem. Phys.* **23**, 356 (1955).
- <sup>59</sup>W. Rżysko, A. Patrykiewicz, and S. Sokołowski, *Phys. Rev. E* **77**, 061602 (2008).
- <sup>60</sup>G. O. Berim and E. Ruckenstein, *J. Chem. Phys.* **126**, 124503 (2007).
- <sup>61</sup>Y. Duda, E. Vakarin, and J. Alejandre, *J. Colloid Interface Sci.* **258**, 10 (2003).
- <sup>62</sup>Y. Tang, Z. Tong, and B. C.-Y. Lu, *Fluid Phase Equilib.* **134**, 21 (1997); **190**, 149 (2001).
- <sup>63</sup>Y. Tang and J.-Z. Wu, *Phys. Rev. E* **70**, 011201 (2004); J. Mi, Y. Tang, C. Zhong, and Y. G. Li, *J. Chem. Phys.* **124**, 144709 (2006); Y. -X. Yu, G. -H. Gao, and X. -L. Wang, *J. Phys. Chem. B* **110**, 14418 (2006); Y. -X. Yu, *J. Chem. Phys.* **131**, 024704 (2009).
- <sup>64</sup>Y. Tang and B. C.-Y. Lu, *Mol. Phys.* **84**, 89 (1995); *Fluid Phase Equilib.* **146**, 73 (1998).
- <sup>65</sup>F. -Q. You, Y. -X. Yu, and G. -H. Gao, *J. Chem. Phys.* **123**, 114705 (2005).
- <sup>66</sup>T. G. Smagala, A. Patrykiewicz, S. Sokołowski, O. Pizio, and W. R. Fawcett, *J. Chem. Phys.* **128**, 024907 (2008).
- <sup>67</sup>S. -J. Lee, Y. Song, and N. A. Baker, *Biophys. J.* **94**, 3565 (2008).